

Different types of Rashba spin-split surface states on Ge(111)

Tetsuya Aruga

Department of Chemistry, Graduate School of Science, Kyoto University, Kyoto 606-8502, Japan

Abstract

In this review article, after a brief account of the early history of the study of the surface Rashba effect is given, a survey is made on an exploration of the Rashba spin-split surface states on a Ge(111) surface. First, the studies on Pb/Ge(111) is shown, which was the first surface with Rashba spin-split *metallic* surface state on a semiconductor established by experiments and first-principles calculation. Second example is Tl/Ge(111), which exhibits valley-like conduction band minimum at the \bar{K} points in the surface Brillouin zone. Due to the symmetry of this surface, spins at the bottom of the valleys are completely polarized parallel to the surface normal. In these two cases, the spin splitting is due to the strong spin-orbit interaction (SOI) in the close proximity to the heavy nuclei at the surfaces. On the other hand, the third example demonstrates that a significant Rashba spin splitting is possible also by SOI at the nuclei of the subsurface Ge atoms. This type of spin-split surface states are believed to be ubiquitous on any types of Ge surfaces as well as at the interfaces between Ge and other materials. A personal view of coming developments in this field is given.

Keywords: Rashba effect, spin orbit interaction, ARPES, SARPES

1. Introduction

The Rashba effect refers usually to a spin orbit interaction (SOI) for electrons moving in a two-dimensional (2D) plane with an electric field perpendicular to it, as described by the Rashba Hamiltonian [1, 2], $\mathcal{H}_R = \alpha_R(\vec{\sigma} \times \vec{p}_{\parallel}) \cdot \hat{e}_z$, where $\vec{\sigma} = (\sigma_x, \sigma_y, \sigma_z)$ denotes the vector of the Pauli spin matrices, $\vec{p} = (p_x, p_y, p_z)$ the momentum operator, \hat{e}_z the unit vector directed normal to the plane, and α_R the Rashba parameter which describes the strength of SOI. Experimentally the Rashba effect was first observed in two-dimensional electron gas (2DEG) confined at GaAs/AlGaAs heterojunctions [3, 4]. The ideas such as that utilizing the Rashba effect to control the spin precession of electrons in 2DEG by electric field [5] have been proposed since then and driving the exploration of the semiconductor-based spin electronics, or, semiconductor spintronics [6].

For the ideal 2D electrons in an electric field perpendicular to the plane, E_z , the Rashba parameter $\alpha_R = \hbar^2 E_z / (4m_e^2 c^2)$ amounts only to $\sim 10^{-3}$ meV \AA^{-1} . However, typical magnitude of α_R for semiconductors such as GaAs and InSb is on the order of 100 meV \AA^{-1} . This clearly indicates that the magnitude of the Rashba SOI is not quantitatively described by the ideal view of 2D free electrons moving in electric field, but is governed by atomic SOI of the constituent atoms of the material that supports the 2D electrons [7, 8]. Since the Fermi wavevector for 2DEG is $\sim 10^{-2}$ \AA^{-1} , the spin splitting at E_F is a few meV, which is much smaller than $k_B T$ at room temperature. Thus the spin-dependent phenomena in these semiconductor heterojunctions can be observed only at

very low temperatures. Semiconductor quantum wells of heavier elements such as HgTe/HgCdTe have Rashba spin splittings up to 30 meV [9].

In 1996, the $\bar{\Gamma}$ surface state on Au(111), which had been known for a decade, was found to be split into two branches [10]. The splitting at E_F was as large as 110 meV, which was ascribed to Rashba SOI. This conclusion was later confirmed by a higher resolution measurement [11], a calculation by full-potential linearized augmented plane wave (LAPW) method [12] and spin- and angle-resolved photoelectron spectroscopy (SARPES) [13]. The work initiated the search for Rashba spin splitting at various surfaces, yielding works on Li/W and Li/Mo(110) [14], H/W(110) [15], the (111), (110) and (100) surfaces of Bi [16], and Gd(0001) [17]. Among them, the surfaces of Bi, which is the heaviest of non-radioactive elements, exhibit spin splittings as large as 300 meV. This splitting may be considered as very large as compared with those in semiconductor heterojunctions. However, the atomic spin-orbit splitting of Bi $6p$ is 2.0 eV, which suggests that the spin splitting on the order of 1 eV should be possible also for conduction bands composed of Bi $6p$.

In 2007, Bi monolayers on Ag(100) surface was found to have a Bi $6p$ -derived surface resonance band, which exhibits Rashba-type splitting on the order of 1 eV [18]. The magnitude of α_R amounts to 3.6 eV \AA^{-1} , which was an order of magnitude larger than those at the surfaces of elemental Bi. This finding indicated that the magnitude of the Rashba spin splitting depends on precise atomic structure of the interface, where the surface state wavefunction is localized, and can be as large as the atomic spin-orbit

splitting. Subsequently, a similar Bi-derived surface band was found for Bi-Ag surface alloy monolayer on Ag(111) with a very similar α_R value of 3.1 eV \AA^{-1} [19]. It was later pointed out that the Rashba parameter approximates to $\int \rho(\mathbf{r})(\partial V/\partial z)d\mathbf{r}$, and therefore the asymmetric charge-density distribution along the surface normal in the vicinity of the nuclei of surface heavy atoms is crucial because the potential gradient $\partial V/\partial z$ is anti-symmetric with respect to the nuclei and is most prominent near the nuclei [8].

These findings suggested that the large Rashba SOI could be realized on the surfaces of semiconductors such as Si and Ge by covering them with a monolayer of heavy elements, which would have significant implications toward the semiconductor spintronics. The possibility was immediately examined for Tl-covered Ge(111) surfaces. Full-potential LAPW method, which had been used in successfully reproducing Rashba spin-split surface state on Au(111) [12], was applied to Ge(111)-(1×1)-Tl [20] [Fig. 1(c)] and Ge(111)-(3×1)-Tl surfaces [21], which showed the large Rashba spin splitting of the Tl-derived surface states on Ge(111) surface. Experimentally, it was shown in 2009 that the Si(111) [22] and Ge(111) [23] surfaces covered with a $(\sqrt{3} \times \sqrt{3})R30^\circ$ -Bi monolayer [Fig. 1(d)] have Rashba spin-split surface states at \bar{M} of the surface Brillouin zone (SBZ). The dispersion and spin splitting of the surface state was again precisely reproduced by a full-potential LAPW calculation [23]. The correspondence between the magnitude of the Rashba parameter and the asymmetry of the charge density distribution along the surface normal in the closest proximity to the Bi nuclei was also verified [23].

The surface state on Si, Ge(111)- $(\sqrt{3} \times \sqrt{3})R30^\circ$ -Bi surfaces is not metallic, because the surface Bi atoms form a trimer structure with saturated valence bonds on these surfaces as shown in Fig. 1(d) [24]. The surfaces, therefore, were not adequate for spin-transport experiment such as intrinsic spin Hall effect (SHE) [25, 26, 27]. However, the finding clearly indicated the possibility of Rashba spin-split surface states on Si and Ge surfaces, which initiated the subsequent studies on the Rashba effect in heavy-element-covered Si and Ge surfaces. While there have been a number of quality works, let us concentrate in this review on some topics related to the Ge(111) surface.

Before going into details of the surface electronic structure, let us show the atomic structures of some of the adsorbate-covered Ge(111) surfaces. Some of them are also formed on Si(111). Clean surfaces of Si(111) and Ge(111) reconstructs into complicated (7×7) and $c(2 \times 8)$ structures. Figure 1(a) shows ideal (1×1) structure. The high-symmetry adsorption sites T_1 (atop), H_3 , and T_4 are shown. Figure 1(b) shows (1×1) -Br surface [28], in which each dangling bond of the topmost Ge atom is terminated by a $4p$ orbital of the Br adatom. On the (1×1) -Tl surface shown in Fig. 1(c) [20], Tl adatoms occupy H_3 sites. Since the $6s^2$ electrons of Tl forms an inert pair, the half-filled surface dangling bonds and the $6p^1$ electrons of Tl atoms

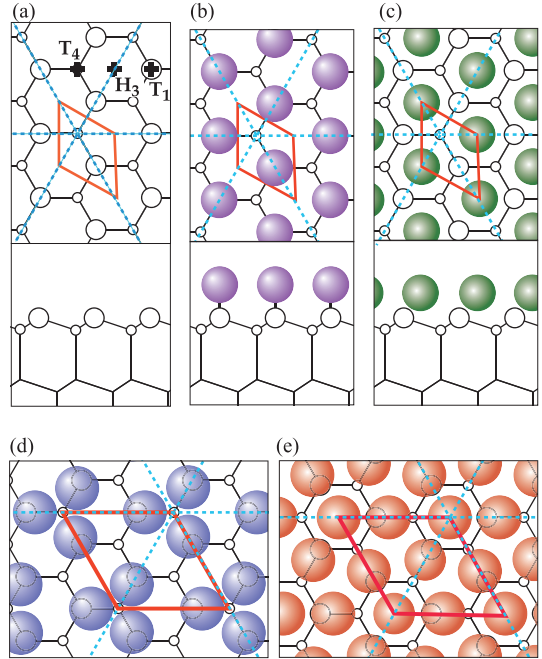


Figure 1: Top and side views of (a) ideal Si(111)- and Ge(111)-(1×1), (b) Si(111)- and Ge(111)-(1×1)-Br, and (c) Si(111)- and Ge(111)-(1×1)-Tl surfaces. Top views of (d) Si(111)- and Ge(111)- $(\sqrt{3} \times \sqrt{3})R30^\circ$ -Bi and (e) Ge(111)- $(\sqrt{3} \times \sqrt{3})R30^\circ$ -Pb surfaces. Rhombi indicate the unit meshes. Dashed lines indicate mirror planes. The structures shown in (a-c) belongs to $p3m1$, while those shown in panels (d, e) belongs to $p31m$ plane group. In panel (a), adsorption sites T_1 , T_4 and H_3 are shown.

form semi-metallic surface states, which will be discussed in Section 3. The Si(111) and Ge(111) surfaces covered with 1 monolayer of Bi atoms form $(\sqrt{3} \times \sqrt{3})R30^\circ$ structure as shown in Fig. 1(d) [24]. While each Bi atom has $6p^3$ valence electrons, one of them are used to terminate the dangling bonds and two others are used form covalent bonds with neighboring Bi atoms, thus forming Bi_3 trimers. As a result, the surface states becomes insulating. On the Ge(111)- $(\sqrt{3} \times \sqrt{3})R30^\circ$ -Pb surface, three Pb atoms per unit cell terminates the surface dangling bonds and a remaining Pb atom per unit cell occupies H_3 sites [36]. It will be shown in Section 2 that this structure gives rise to a nearly-free-electron surface state localised in the Pb monolayer. In Fig. 1 are also shown mirror planes on these surfaces. In the $(\sqrt{3} \times \sqrt{3})R30^\circ$ structures shown in Fig. 1(d,e), the mirror planes are parallel with the sides of the unit mesh, while the mirror planes are not parallel with the sides in the (1×1) structures shown in Fig. 1(a-c). This has an interesting relevance to the spin splitting on these surfaces, which will be discussed in Section 3.

2. Nearly-free-electron surface states on Pb/Ge(111)

In order to establish metallic surface state spin-split by the Rashba effect on semiconductor surfaces, the Si and Ge(111) surfaces covered with heavy elements such as

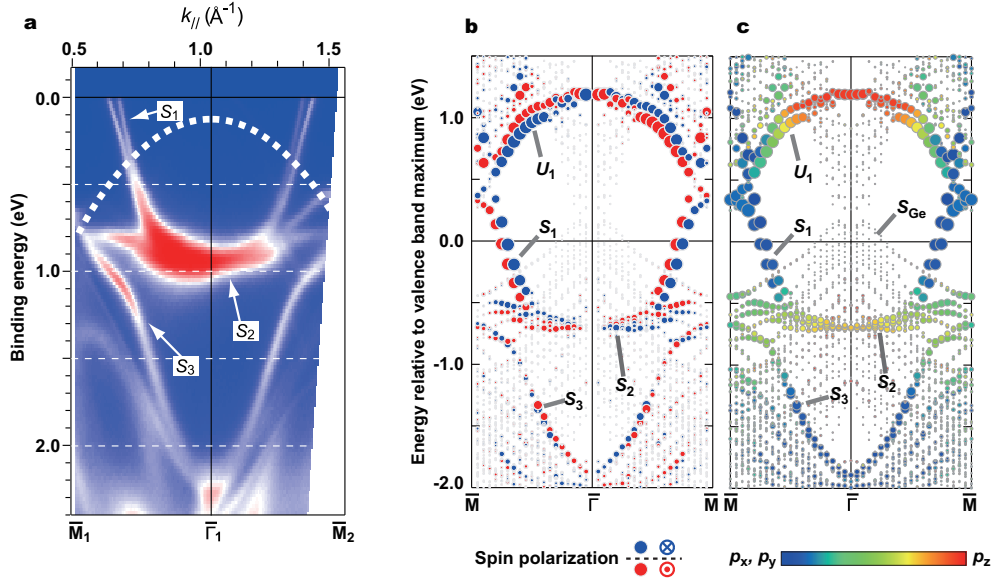


Figure 2: Measured and computed energy-band structure of Ge(111)- $\beta(\sqrt{3} \times \sqrt{3})R30^\circ$ -Pb. (Reproduced from Ref. [34].) (a) Experimental energy-band dispersion measured by angle-resolved photoelectron spectroscopy (ARPES) at 30 K. The dashed line indicates the upper edge of the bulk bands of Ge. (b) Computed energy-band structure for the Ge(111)- $\beta(\sqrt{3} \times \sqrt{3})R30^\circ$ -Pb surface. The radii of the blue (red) circles are proportional to the net contribution of the Pb 6p with spin up (down). (c) Computed energy-band structure with relative contribution of Pb $6p_x p_y$ and $6p_z$ shown by color scale. The sizes of the circles are proportional to the total contribution of Pb 6p.

^{79}Au , ^{81}Tl , ^{82}Pb and ^{83}Bi were considered as candidates. As already mentioned, Bi/Si(111) and Bi/Ge(111) at a coverage of 1 have qualitatively the same atomic structure and exhibit almost identical, semiconducting surface states. On the other hand, the structural phases of Pb/Ge(111) and Pb/Si(111) are different. The Pb-covered Si(111) surface was known to exhibit a variety of structural phases which are often very complicated, in particular, at coverages near and higher than 1 [29, 30, 31, 32]. The electronic structure of some of the high-coverage phases were found to be metallic, but the Fermi contours were complicated [33].

At coverages higher than 1, the Pb/Ge(111) surface forms only the $\beta(\sqrt{3} \times \sqrt{3})R30^\circ$ phase at a coverage of $4/3$ [Fig. 1e)]. The first experimental identification of the metallic surface state that is spin split by Rashba SOI was achieved for the Ge(111)- $\beta(\sqrt{3} \times \sqrt{3})R30^\circ$ -Pb surface [34].

Figure 2 shows the measured and computed energy-band structure of the Pb/Ge(111)- $\beta\sqrt{3}$ surface. The experimental band suggests that a nearly-free-electron parabolic band is hybridized with a almost flat band (S_2) to yield a upper (S_1) and a lower (S_3) branch. The S_1 band was found to be split into two branches, which was studied by SARPES and was found to be spin-polarized to the directions opposite to each other as expected from the Rashba Hamiltonian [34]. The Rashba parameter was slightly energy dependent and was 0.35 eV \AA at E_F . The spin splitting at E_F amounted to 200 meV, which is an order of magnitude larger than the thermal energy at room temperature.

The calculation, which was carried out by using full-potential LAPW code [35], reproduced the experimental

band dispersion and the spin polarization quantitatively. Moreover, the calculation revealed the orbital character of the surface states as shown in Fig. 2(c). The S_1 band is composed mostly of Pb $6p_x p_y$ and confined in the Pb monolayer. The S_2 band is essentially of a bonding character between the dangling bonds of the topmost Ge atoms and the Pb atoms near the atop (T_1) sites. The unoccupied U_1 band around $\bar{\Gamma}$ corresponds to the $6p_z$ orbital of the Pb atoms at H_3 sites [36].

The Rashba spin-split metallic states on semiconductor surface is interesting with respect not only to the spin transport phenomena such as SHE, but also to usual electric conductance since the large Rashba spin splitting may alter the scattering process of conduction electrons. A recent experiment indicated unusual electrical transport on this surface [37], which probably is related to the large Rashba spin splitting of the metallic surface state.

3. Uniaxially spin-polarized \bar{K} surface states on Tl/Ge(111)

The Rashba spin-split states are always degenerated at $\bar{\Gamma}$, which gives rise to the characteristic band crossing of the spin-split pair at $\bar{\Gamma}$. Similar band crossing is also observed at \bar{M} of the hexagonal lattice such as Ge(111)- $(\sqrt{3} \times \sqrt{3})R30^\circ$ -Bi [23], because of the time reversal symmetry of this point. For the $(\sqrt{3} \times \sqrt{3})R30^\circ$ surface, the band crossing is also observed at \bar{K} point whereas there is no time reversal symmetry [38]. The crossing in this case is due to the C_{3v} point-group symmetry of the \bar{K} point for the $(\sqrt{3} \times \sqrt{3})R30^\circ$ structure that belongs to $p31m$ plane

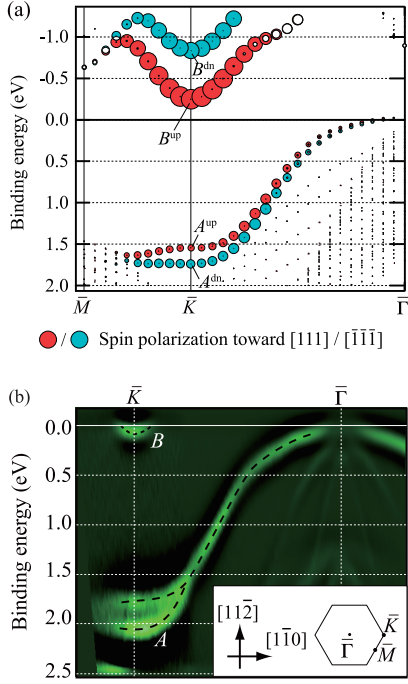


Figure 3: Measured and computed energy-band structure of Ge(111)-(1 × 1)-Tl. (Reproduced from Ref. [41].) (a) Computed energy-band structure for the as-prepared Ge(111)-α(1 × 1)-Tl surface. The radii of the red (blue) circles are proportional to the net contribution of Tl with spin oriented parallel (anti-parallel) to the surface normal. (b) Experimental energy-band dispersion of the Tl-doped Ge(111)-β(1 × 1)-Tl measured by ARPES.

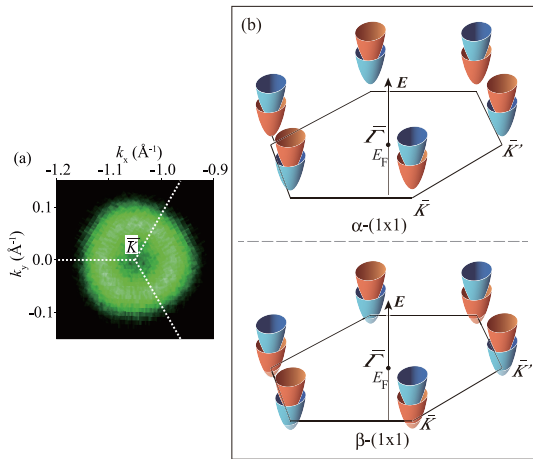


Figure 4: (a) The Fermi contour around \bar{K} for the $\beta(1 \times 1)$ surface measured by ARPES. (Reproduced from Ref. [41].) (b) Schematic structure of the B_{up} and B_{dn} bands in the α and β phases.

group [See Fig. 1(d)]. On the other hand, the (1 × 1)-Tl structure belongs to $p3m1$ plane group [Fig. 1(c)], in which case the \bar{K} point has a C_3 point-group symmetry. In this case, the spin-split pair is not degenerated [39].

The Pauli spin-orbit interaction is decomposed into two terms:

$$\begin{aligned} \mathcal{H}_{\text{SO}} &\propto \vec{\sigma} \cdot (\vec{\nabla}V \times \vec{p}) \\ &= \frac{\partial V}{\partial z} (p_x \sigma_y - p_y \sigma_x) + \left(\vec{\nabla}_{\parallel} V \times \vec{p}_{\parallel} \right) \sigma_z, \end{aligned}$$

where V denotes the Coulomb potential, $\vec{\nabla}_{\parallel} = \vec{e}_x(\partial/\partial x) - \vec{e}_y(\partial/\partial y)$, and $\vec{p}_{\parallel} = (p_x, p_y, 0)$. The first term corresponds to the usual Rashba term, which describes the surface parallel spin polarization induced by surface normal potential gradient. The second term describes the surface-normal spin polarization due to the in-plane potential gradient. At the \bar{K} points in the 2D Brillouin zone of the hexagonal lattice, the first term vanishes and only the second term, which corresponds to the surface normal spin polarization, is expected. Therefore, the spin polarization along the surface normal should be realized at the \bar{K} point on the (1 × 1)-Tl surfaces.

The Tl-adsorbed Ge(111) surface exhibits one-dimensional (3 × 1) structure [21, 40] as well as isotropic (1 × 1) structure [20]. For the (1 × 1)-Tl surface, the breakdown of the degeneracy was first acknowledged in 2007 by a LAPW calculation [20].

Experimentally, it was found that the adsorption of a small amount of Tl on top of the ideal (1 × 1)-Tl surface results in doping of electrons to the surface electronic states, and converts the Fermi surface from the hole pocket at $\bar{\Gamma}$ to the electron pockets at \bar{K} [41]. The ideal and Tl-doped surfaces were denoted as $\alpha(1 \times 1)$ and $\beta(1 \times 1)$, respectively.

Figure 3(a) shows the band structure of Ge(111)-α(1 × 1)-Tl computed by the LAPW method. Two pairs of surface states, A and B , are found. The surface state A forms a hole pocket around $\bar{\Gamma}$, which was confirmed by ARPES experiment [41]. The A band disperses downward from $\bar{\Gamma}$ to \bar{K} . It has strong in-plane spin orientation, characteristic to the normal Rashba spins, near the $\bar{\Gamma}$ point, but changes its spin orientation to the surface normal upon approaching \bar{K} . Note that the size of the circles in Fig. 3(a) is proportional to the contribution of Tl with spin oriented normal to the surface. The unoccupied surface state B is found around \bar{K} and is spin polarized completely along the surface normal at \bar{K} . The electron doping by addition of a small amount of Tl causes the disappearance of the hole pocket at $\bar{\Gamma}$ and the concomitant appearance of electron pockets at the \bar{K} points in the $\beta(1 \times 1)$ surface as shown in Fig. 3(b).

Fermi contour for the $\beta(1 \times 1)$ -Tl surface measured by ARPES is shown in Fig. 4(a). Also, a schematic of the B band in the α and β phases is shown in Fig. 4(b). The spin polarization at a pair of opposite \bar{K} points with respect to $\bar{\Gamma}$ is reversed. The overall spin texture is as shown in Fig. 4(b). The spin structure of the $\alpha(1 \times 1)$ surface resembles

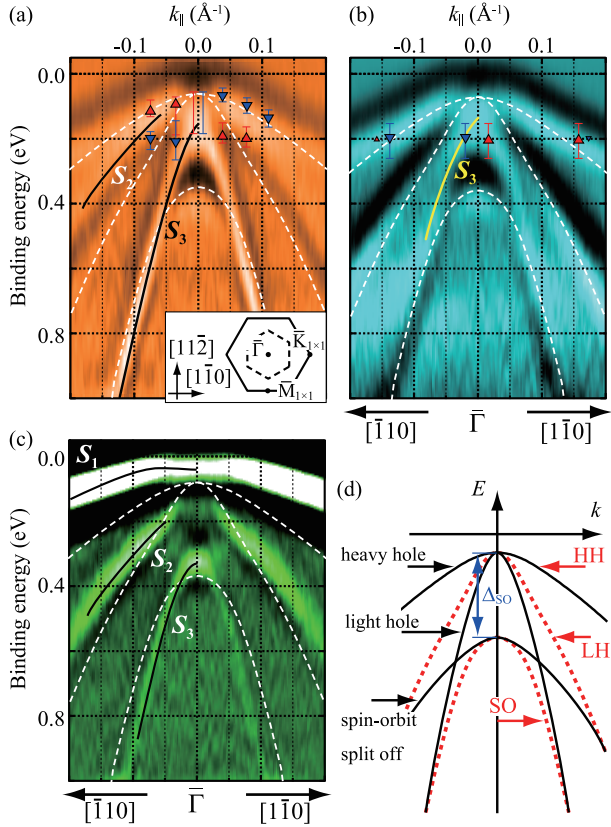


Figure 5: Second-derivative ARPES images for (a) Ge(111)-($\sqrt{3} \times \sqrt{3}$) $R30^\circ$, (b) Ge(111)-(1 \times 1)-Br, and (c) Ge(111)-(1 \times 1)-Tl. (d) Schematic of bulk Ge band structure. $\Delta_{\text{SO}} = 0.29$ eV. Panel (a) was reproduced from Ref. [44]. Panels (b), (c), and (d) were reproduced from Ref. [45]. Dashed lines indicate the upper edges of the HH, SO, and LH bands, which were calculated by a tight-binding method with parameters fitted to the bulk bands. Triangle markers in (a) and (b) show the spin polarization measured by SARPES [44].

those of MoS₂ and WS₂, suggesting that it is possible to selectively populate the electrons with particular spin polarization by optically pumping with circularly polarized light [42, 43]. On the other hand, the $\beta(1 \times 1)$ surface has a spin-polarized metallic surface states, suggesting that it is usable to study spin transport phenomena.

4. $\bar{\Gamma}$ surface states derived from subsurface Ge orbitals

Since the discovery of the surface Rashba effect on Au(111) [10], efforts had been paid to study the surfaces containing heavy elements in the 6th row of the periodic table. In 2010, however, the spin-polarized surface states localized in subsurface layers of the Ge(111)-($\sqrt{3} \times \sqrt{3}$) $R30^\circ$ -Bi surface [Fig. 1(d)] was discovered and the spin polarization was ascribed to the Rashba SOI at the nuclei of subsurface Ge atoms [44]. Similar spin-polarized surface states were identified also on Ge(111)-(1 \times 1)-Br [Fig. 1(b)] [28], Ge(111)-(1 \times 1)-Tl [Fig. 1(c)] [45], and Ge(111)-($\sqrt{3} \times \sqrt{3}$) $R30^\circ$ -Pb surfaces [Fig. 1(e)] [46]. Since Br is in the fourth row, the same as Ge, in the periodic table,

it is clear that the heavy elements that cover the surface are not essential to the spin polarization observed on these surfaces.

Figure 5 shows the ARPES data around $\bar{\Gamma}$ for the Bi/Ge(111), Br/Ge(111) and Tl/Ge(111) [44, 28, 45]. For all the three cases, the band denoted S_3 is running along the bulk SO band edge at $k_{\parallel} > 0.05 \text{ \AA}^{-1}$. The S_3 band disperses into the bulk spin-orbit gap at $k_{\parallel} < 0.05 \text{ \AA}^{-1}$, indicating that this is a surface state. Also the bands running slightly below the HH band edge, denoted S_2 , is found on Bi/Ge(111) and Tl/Ge(111). The S_1 band observed only on Tl/Ge(111) is due to the weak hybridization between Ge $3p_z$ dangling bonds and the $6p_z$ orbitals of Tl occupying the T_4 sites. SARPES experiments revealed that these surface states are spin polarized as indicated by red and blue triangles. The spin polarization is reversed with respect to $\bar{\Gamma}$, suggesting that it is due to the Rashba SOI.

Figure 6 shows the band structure calculated by the full-potential LAPW method [28, 45]. In the upper panels (a-c), the electronic states that have a large contribution of the subsurface Ge layers are indicated by large circles. The surface states, S_1 , S_2 , and S_3 , observed by ARPES is reproduced well by the calculated states, S_a^\pm , S_b^\pm , and S_c^\pm . The lower panels (d-f) shows the spin polarization toward the directions expected for the Rashba effect is shown by large circles. The spin polarization observed by SARPES is also well reproduced. Note that the S_a^\pm bands in Tl/Ge(111) are spin polarized parallel to the surface near $\bar{\Gamma}$ due to the normal Rashba effect, while the spin orientation changes to the surface normal upon approaching \bar{K} . Note also that the S_c^+ and S_c^- bands are not degenerate at $\bar{\Gamma}$, while these two bands appear to be a spin-split pair.

Figure 7 shows the depth profile of the partial charge distribution of the states S_b and S_c indicated by the arrows in Fig. 6(d) for Bi/Ge(111). The partial charge is calculated as $|\langle \phi_{lm}^i, \uparrow | \Psi_{k_{\parallel}, E} \rangle|^2$, where $|\phi_{lm}^i, \uparrow\rangle$ represents each atomic orbital in the i th layer and $|\Psi_{k_{\parallel}, E}\rangle$ the eigenfunction for the calculated state at (k_{\parallel}, E) . Note that, since the “atomic orbitals” are defined only within atomic spheres and the wavefunctions in the interstitial space is described by plane waves in the LAPW method, the partial charge summed up for all the atoms is less than unity. Both states has a similar distribution, which has a broad maximum at around the fifth Ge layer and gradually decay upon going into the bulk. The distribution implies that these surface states, S_2 (S_b) and S_3 (S_c) are formed from the bulk states LH and SO, respectively, due to the perturbation induced by the truncation of the bulk translational symmetry at the surface. The S_1 (S_a) band in Tl/Ge(111) is the same as the A band in Fig. 3, which is formed by the weak hybridization between Ge $4p_z$ with the $6p_z$ orbitals of the Tl atoms at H_3 sites. For Bi/Ge(111) and Br/Ge(111), since the adatoms occupy the T_1 sites, the Ge $4p_z$ orbitals strongly interact with the p_z orbitals of the adsorbates and form flat bands with bonding and antibonding characters

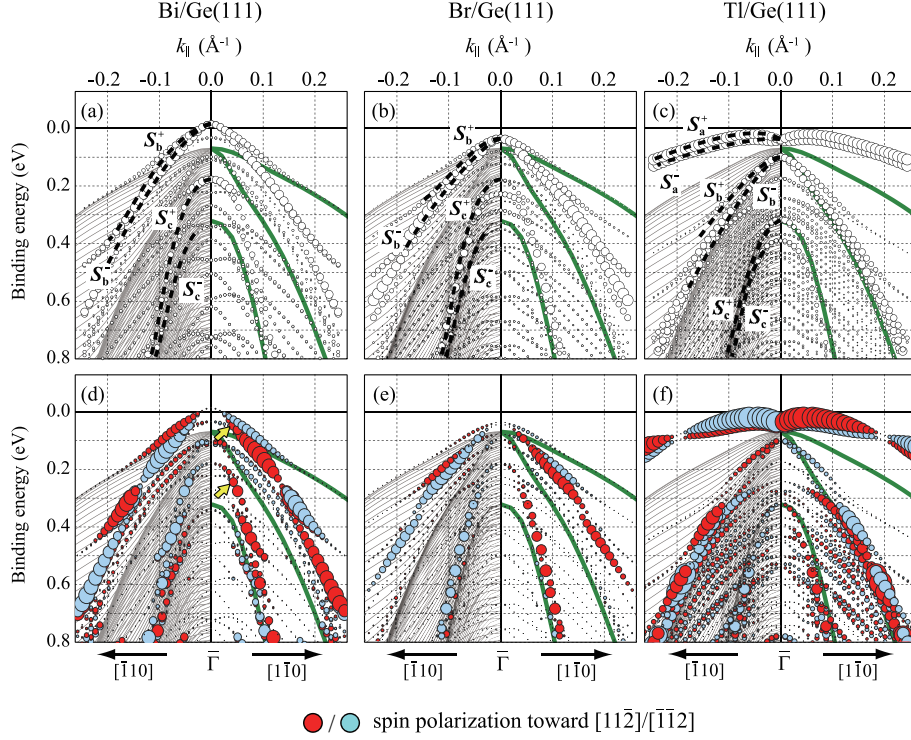


Figure 6: Calculated band structures for (a,d) Ge(111)- $(\sqrt{3} \times \sqrt{3})R30^\circ$ -Bi, (b,e) Ge(111)-(1 \times 1)-Br, and (c,f) Ge(111)-(1 \times 1)-Tl. The radii of the circles in panels (a-c) indicate total contribution of the subsurface layers, while those in panel (d-e) show net spin polarization. Thin lines in the left halves show bulk valence bands. Thick lines in the right halves show the upper edges of the HH, LH, and SO bands. Panel (e) was reproduced from Ref. [28] and panels (a), (b), (c), (d) and (f) were reproduced from Ref. [45].

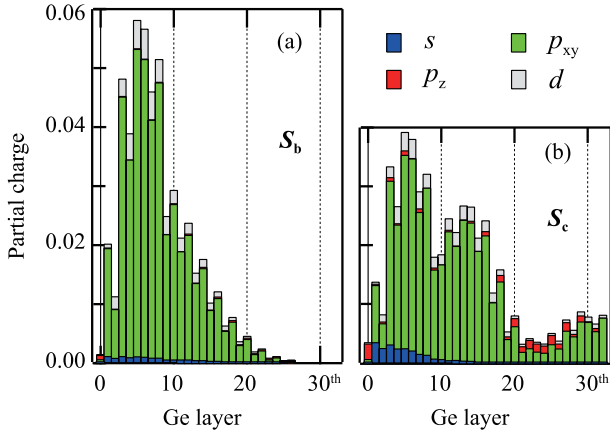


Figure 7: Layer- and spin-resolved partial charges of surface states S_b and S_c of Ge(111)- $(\sqrt{3} \times \sqrt{3})R30^\circ$ at the states indicated by the arrows in Fig. 6(d). The zeroth layer corresponds to the Bi layer. Reproduced from Ref. [45].

at 0.5–1.0 eV below and above E_F . Hence the subsurface states are predominantly of the Ge $4p_x p_y$ character as indicated in Fig. 7. All of these states are not bulk states but are localized in the surface/subsurface region, the states are spin-split due to the Rashba SOI.

Since the surface states localized in subsurface layers originate from the bulk states which are perturbed by the truncation of the bulk translational symmetry, similar sub-

surface states should be formed even on clean Ge(111) surface. However, since the clean Ge(111) surface is reconstructed in $c(2 \times 8)$ periodicity, it is not very easy to identify the subsurface states and their spin polarization. A recent full-potential LAPW calculation for a hypothetical Ge(111)-(1 \times 1) surface and Ge(111)-(1 \times 1)-H surface indicates the existence of spin-polarized subsurface states [47].

The lifting of the degeneracy at $\bar{\Gamma}$ of the S_c^+ and S_c^- branches can be understood as the “partner-switching” similar to that in topological insulators. Since these branches are resonances within bulk continua, each of them can change its partner at $\bar{\Gamma}$ to another band which may be a bulk band [45].

5. Summary

During the past decade, the electronic structure of the Rashba spin-split states on semiconductor surfaces has been established by spectroscopic means such as ARPES and SARPEs and by theories and computations. A next important topic along this line will be transport phenomena, including spin transport such as SHE, spin filters [48], and spin light-emitting diodes [49]. At the moment, the Ge(111)- $\beta(\sqrt{3} \times \sqrt{3})R30^\circ$ -Pb surface is probably a nice candidate to study spin transport phenomena on surfaces, since it has a nearly-free-electron band with a large spin splitting and a very good surface order. The surface shows

no phase transition down to 10 K [37], which is important for low temperature spin transport experiments. The peculiar spin texture of the Ge(111)-(1 × 1)-Tl surface is useful for the optoelectronic studies. Optical pumping with circularly polarized light can be used to selectively populate the conduction band with uniquely spin-polarized electrons.

The third topic in this review, the spin-polarized sub-surface states may have a most significant implication for the forthcoming semiconductor spintronics. Since the sub-surface states are derived from the corresponding bulk states due to the truncation of the bulk periodicity, these are essentially interface states. This suggests that similar spin-split states should be formed at the heterointerface between bulk Ge with other solids such as Si. This has an important consequence. Usually, metal-covered semiconductor surfaces prepared in ultrahigh vacuum chambers are very sensitive to the exposure to gasses. Hence transport experiments should be conducted *in vacuo*. On the other hand, if the spin-split states are formed at the heterointerface of, for instance, Ge and Si, it should be possible to bring the sample out of the vacuum chamber and carry out spin transport experiments such as intrinsic SHE under ambient conditions. If the interface state that is spin-split by ~ 100 meV is achieved at semiconductor heterojunctions, it would bring a breakthrough toward the semiconductor spintronics.

References

- [1] É. I. Rashba, *Fiz. Tverd. Tela (Leningrad)* 2 (1960) 1224 [*Sov. Phys. Solid State* 2 (1960) 1109].
- [2] Yu. A. Bychkov and É. I. Rashba, *Pis'ma Zh. Eksp. Teor. Fiz.* 39 (1984) 66 [*JETP Lett.* 39 (1984) 78].
- [3] H. L. Stormer, Z. Shlesinger, A. Chang, D. C. Tsui, A. C. Gossard and W. Wiegmann, *Phys. Rev. Lett.* 51 (1983) 126.
- [4] D. Stein, K. v. Klitzing and G. Weimann, *Phys. Rev. Lett.* 51 (1983) 130.
- [5] S. Datta and B. Das, *Appl. Phys. Lett.* 56 (1990) 665.
- [6] D. D. Awschalom and M. E. Flatté, *Nat. Phys.* 3 (2007) 153.
- [7] L. Petersen and P. Hedegard, *Surf. Sci.* 459 (2000) 49.
- [8] M. Nagano, A. Kodama, T. Shishidou and T. Oguchi, *J. Phys.: Condens. Matter* 21 (2009) 064239.
- [9] Y. S. Gui, C. R. Becker, N. Dai, J. Liu, Z. J. Qiu, E. G. Novik, M. Schäfer, X. Z. Shu, J. H. Chu, H. Buhmann and L. W. Molenkamp, *Phys. Rev. B* 70 (2004) 115328.
- [10] S. LaShell, B. A. McDougall and E. Jensen, *Phys. Rev. Lett.* 77 (1996) 3419.
- [11] F. Reinert, G. Nicoley, S. Schmidt, D. Ehm and S. Hüfner, *Phys. Rev. B* 63 (2001) 115415.
- [12] G. Nicoley, F. Reinert, S. Hüfner and P. Blaha, *Phys. Rev. B* 65 (2002) 033407.
- [13] M. Hoesch, M. Muntwiler, V. N. Petrov, M. Hengsberger, L. Patthey, M. Shi, M. Falub, T. Greber and J. Osterwalder, *Phys. Rev. B* 69 (2004) 241401(R).
- [14] E. Rotenberg, J. W. Chung and S. D. Kevan, *Phys. Rev. Lett.* 82 (1999) 4046.
- [15] M. Hochstrasser, J. G. Tobin, E. Rotenberg and S. D. Kevan, *Phys. Rev. Lett.* 89 (2002) 216802.
- [16] Y. M. Koroteev, G. Bihlmayer, J. E. Gayone, E. V. Chulkov, S. Blügel, P. M. Echenique and P. Hofmann, *Phys. Rev. Lett.* 93 (2004) 046403.
- [17] O. Krupin, G. Bihlmayer, K. Starke, S. Gorovikov, J. E. Prieto, K. Döbrich, S. Blügel and G. Kaindl, *Phys. Rev. B* 71 (2005) 201403(R).
- [18] T. Nakagawa, O. Ohgami, Y. Saito, H. Okuyama, M. Nishijima, and T. Aruga, *Phys. Rev. B* 75 (2007) 155409.
- [19] C. R. Ast, J. Henk, A. Ernst, L. Moreschini, M. C. Falub, D. Pacilé, P. Bruno, K. Kern and M. Grioni, *Phys. Rev. Lett.* 98 (2007) 186807.
- [20] S. Hatta, C. Kato, N. Tsuboi, S. Takahashi, H. Okuyama, T. Aruga, A. Harasawa, T. Okuda, and T. Kinoshita, *Phys. Rev. B* 76 (2007) 075427.
- [21] S. Hatta, T. Aruga, C. Kato, S. Takahashi, H. Okuyama, A. Harasawa, T. Okuda, and T. Kinoshita, *Phys. Rev. B* 77 (2008) 245436.
- [22] I. Gierz, T. Suzuki, E. Frantzeskakis, S. Pons, S. Ostanin, A. Ernst, J. Henk, M. Grioni, K. Kern and C. R. Ast, *Phys. Rev. Lett.* 103 (2009) 046803.
- [23] S. Hatta, T. Aruga, Y. Ohtsubo and H. Okuyama, *Phys. Rev. B* 80 (2009) 113309.
- [24] Y. Ohtsubo, S. Hatta, M. Iwata, K. Yaji, H. Okuyama and T. Aruga, *J. Phys.: Condens. Matter* 21 (2009) 405001.
- [25] M. I. D'yakonov and V. I. Perel, *Zh. Eksp. Teor. Fiz. Pis'ma Red.* 13 (1971) 657 [*JETP Lett.* 13 (1971) 467].
- [26] J. E. Hirsch, *Phys. Rev. Lett.* 83 (1999) 1834.
- [27] Y. Kato, R. C. Meyers, A. C. Gossard and D. D. Awschalom, *Science* 306 (2004) 1910.
- [28] Y. Ohtsubo, S. Hatta, N. Kawai, A. Mori, Y. Takeuchi, K. Yaji, H. Okuyama, and T. Aruga, *Phys. Rev. B* 86 (2012) 165325.
- [29] G. Le Lay, M. Abraham, A. Kahn, K. Hricovini and J. E. Bonnet, *Phys. Scr.* T35 (1991) 261.
- [30] L. Seehofer, G. Falkenberg, D. Daboul and R. L. Johnson, *Phys. Rev. B* 51 (1995) 13503.
- [31] K. Horikoshi, X. Tong, T. Nagao and S. Hasegawa, *Phys. Rev. B* 60 (1999) 13287.
- [32] M. Hupalo, J. Schmalian and M. C. Tringides, *Phys. Rev. Lett.* 90 (2003) 216106.
- [33] W. H. Choi, H. Koh, E. Rotenberg and H. W. Yeom, *Phys. Rev. B* 75 (2007) 075329.
- [34] K. Yaji, Y. Ohtsubo, S. Hatta, H. Okuyama, K. Miyamoto, T. Okuda, A. Kimura, H. Namatame, M. Taniguchi, and T. Aruga, *Nat. Commun.* 1 (2010) 17.
- [35] P. Blaha, K. Schwarz, G. K. H. Madsen, D. Kvasnicka and J. Luiz, *WIEN2k, An Augmented Plane Wave + Local Orbitals Program for Calculating Crystal Properties* (Karlheinz Schwarz, Techn. Universität Wien, Austria, 2001) ISBN-3-9501031-1-2.
- [36] K. Yaji, S. Hatta, T. Aruga, and H. Okuyama, *Phys. Rev. B* 86 (2012) 235317.
- [37] S. Hatta, T. Noma, H. Okuyama and T. Aruga, to be published.
- [38] K. Sakamoto, H. Kakuta, K. Sugawara, K. Miyamoto, A. Kimura, T. Kuzumaki, N. Ueno, E. Annese, J. Fujii, A. Kodama, T. Shishidou, H. Namatame, M. Taniguchi, T. Sato, T. Takahashi and T. Oguchi, *Phys. Rev. Lett.* 103 (2009) 156801.
- [39] T. Oguchi and T. Shishidou, *J. Phys.: Condens. Matter* 21 (2009) 092001.
- [40] S. Hatta, R. Ohtomo, C. Kato, O. Sakata, H. Okuyama and T. Aruga, *J. Phys.: Condens. Matter* 20 (2008) 395226.
- [41] Y. Ohtsubo, S. Hatta, H. Okuyama, and T. Aruga, *J. Phys.: Condens. Matter* 24 (2012) 092001.
- [42] H. Zeng, J. Dai, Y. Wang, D. Xial and X. Cui, *Nature Nanotech.* 7 (2012) 490.
- [43] K. F. Mak, K. He, J. Shan and T. F. Heinz, *Nature Nanotech.* 7 (2012) 494.
- [44] Y. Ohtsubo, S. Hatta, K. Yaji, H. Okuyama, K. Miyamoto, T. Okuda, A. Kimura, H. Namatame, M. Taniguchi, and T. Aruga, *Phys. Rev. B* 82 (2010) 201307(R).
- [45] Y. Ohtsubo, K. Yaji, S. Hatta, H. Okuyama, and T. Aruga, *Phys. Rev. B* 88 (2013) 245310.
- [46] K. Yaji, Y. Ohtsubo, S. Hatta, H. Okuyama, R. Yukawa, I. Matsuda, P. Le Fèvre, R. Bertran, A. Taleb-Ibrahimi, A. Kak-

- izaki and T. Aruga, J. Electron Spectrosc. Relat. Phenom., *in this issue* (2014).
- [47] T. Aruga, S. Hatta, and H. Okuyama, *in preparation*.
- [48] Y. K. Koga, J. Nitta, H. Takayanagi and S. Datta, Phys. Rev. Lett. 88 (2002) 126601.
- [49] B. T. Jonker, Y. D. Park, B. R. Bennet, H. D_i Cheong, G_i Kioseoglou and A. Petrou, Phys. Rev. B 62 (2000) 8180.